Available online at www.sciencedirect.com
ScienceDirect
Journal of Sound and Vibration 324 (2009) 387–407
JOURNAL OF SOUND AND VIBRATION
www.elsevier.com/locate/jsvi

Comprehensive stability analysis of disc brake vibrations including gyroscopic, negative friction slope and mode-coupling mechanisms

Jaeyoung Kang[a,b,*,1], Charles M. Krousgrill[a], Farshid Sadeghi[a]

[a]School of Mechanical Engineering, 585 Purdue Mall, Purdue University, West Lafayette, IN 47907-2088, USA
[b]Division of Mechanical and Automotive Engineering, College of Engineering, Kongju National University, 275 Budae-Dong, Cheonan-Si, Chungnam, 330-717, Korea

Received 18 July 2008; received in revised form 22 January 2009; accepted 29 January 2009
Handling Editor C.L. Morfey
Available online 12 March 2009

Abstract

The current study investigates the disc brake squeal by using an annular disc in contact with two pads subject to distributed friction stresses. The disc and pads are modeled as rotating annular and stationary annular sector plates, respectively. Friction stress is described on the deformed disc surface as distributed non-conservative friction-couples and frictional follower forces. From disc doublet-mode and multiple-mode models, the mode-coupling mechanism influenced by disc rotation is examined. In automotive applications, the frictional mode-coupling resulting from friction couple is shown to be the major mechanism for dynamic destabilization, whereas the effects of disc rotation on flutter destabilization are found to be small. On the verge of stop, however, the rotation effects effectively stabilize the steady sliding. This comprehensive brake model has shown that there is a speed corresponding to maximum squeal propensity for each flutter mode.

1. Introduction

Brake squeal vibration has been a challenging problem to solve in automotive industry. Many researchers have investigated mechanisms for the generation of squeal; however, a complete explanation of squeal generation has not yet been available due to complexity of the problem. One common direction of study in brake squeal has been the numerical linear stability analysis predicting the instabilities of the system equilibrium.

The friction-engaged disc brake model can be discretized by means of the assumed modes method or the finite element (FE) method resulting in the finite degree-of-freedom matrix form of the equations of motion

*Corresponding author at: Division of Mechanical and Automotive Engineering, College of Engineering, Kongju National University, 275 Budae-Dong, Cheonan-Si, Chungnam, 330-717, Korea. Tel.: +82 41 521 9263.
E-mail address: jkang@kongju.ac.kr (J. Kang).
[1]He is currently an assistant professor at Kongju National University in Korea.

0022-460X/$ - see front matter © 2009 Elsevier Ltd. All rights reserved.
doi:10.1016/j.jsv.2009.01.050

(Kinkaid et al. [1] and Ouyang et al. [2]):

$$\mathbf{M}\ddot{\mathbf{x}} + (\mathbf{G} + \mathbf{D})\dot{\mathbf{x}} + (\mathbf{K_s} + \mathbf{K_{ns}})\mathbf{x} = \mathbf{0}, \tag{1}$$

where **M**, **G** and **D** are the symmetric mass, skew-symmetric gyroscopic and symmetric damping matrices, respectively. $\mathbf{K_s}$ and $\mathbf{K_{ns}}$ are the symmetric stiffness and non-symmetric frictional mode-coupling matrices, respectively, for the system [2].

Basically, the approach on the stability criteria of the linearized equations of motion is based on the trace of the system eigenvalues. The general stability theories on the dynamic system under general loading cases have been introduced in Refs. [3–7]. The analytical and numerical stability results on the two rigid rotating discs in contact under damping, gyroscopic and circulatory loading have been introduced as well [8]. However, a comprehensive analytical formulation on the disc brake application has not been proposed before due to its geometric and dynamic complexity.

In the disc brake literature, $\mathbf{K_{ns}}$ has been constructed from two non-conservative friction loadings: the frictional follower force [9–11] and the friction couple [12–15]. For comparison of these quantities, Flint and Hulten [15] used a flexible beam in contact with two flexible pads for a disc brake modeling and investigated the contribution of the two friction types. Heilig and Wauer [16] examined the contribution of the two friction types from a disc brake model with a rotating ring in contact with two-point masses. They all concluded that frictional follower force in application to disc brake system has an insignificant influence on response stability. Another modeling aspect influencing the elements of $\mathbf{K_{ns}}$ is the choice of area loaded by friction stresses: point contact ([9,14,16,17]) vs. distributed-loaded contact ([11–13,15,18–24]). The squeal propensity of the distributed-loaded contact model was examined and it was concluded that the contact area (particularly, contact span angle) strongly influences the flutter instability in Ref. [23]. The validity of the point contact model for brake squeal mechanism will be later addressed in this paper.

The gyroscopic terms $\mathbf{G}\dot{\mathbf{x}}$ are typically ignored on the basis that brake squeal vibrations normally occur at low operational speeds. However, the work by Ouyang et al. introduced the effect of moving contact loads ([14,18]) or the gyroscopic effect [19]. From these models, they concluded that the instability of disc brake is dependent of rotation speed. Heilig and Wauer [16] and Hochlenert et al. [17] investigated the gyroscopic effects from a rotating disc in point-contact with two stationary pads. They provided a consistent conclusion that rotation speed influences the destabilization of the disc brake system. However, the analytical explanation on gyroscopic effect as a squeal propensity was not provided in detail.

Lastly, the $\mathbf{D}\dot{\mathbf{x}}$ terms take on the role of system damping, either in stabilizing or destabilizing manner. The damping types used in the previous disc brake models are the positive structural damping, the negative damping obtained from the linearization of friction-speed curve, and the positive radial frictional damping. Hochlenert et al. [17] included the frictional damping from the radial component of friction stresses and showed that the system damping decreases at a rate of $1/\Omega$, where Ω is the rotation rate. Kung et al. [20] indicated that the negative damping stemming from the negative slope of friction coefficient contributes to the destabilization of the brake system at low speeds.

As mentioned above, many models and results on brake squeal have been provided. However, disc brake squeal still remains an elusive problem. One major limitation at this point is that the models do not provide a comprehensive explanation on brake squeal mechanisms. For example, the mode-merging approach has been useful to demonstrate the mode-coupling instability as one squeal mechanism at the static steady-sliding equilibrium, but limited in investigating squeal propensity for disc rotation speed. On the other hand, the rotating disc models have focused on the rotation effect on the equilibrium instability with the lack of explanation on mode-coupling mechanism. The motivation of this study is to resolve these limitations for understanding disc brake squeal mechanism.

The goal of this paper is to describe brake squeal mechanisms using a comprehensive dynamic model. The stability of the homogeneous solutions of Eq. (1) is interpreted in terms of binary flutter resulting from the modal interaction of two closely spaced modes [21–24]. The disc brake system is modeled as a rotating disc and two flexible pads, where the linearized contact model for a thin plate [17] is utilized. The analytical and numerical investigations enable us to evaluate the parametric contribution to the dynamic instability and the corresponding squeal mechanisms. Moreover, the results of the comprehensive model provide the physical background for the further approximations and simplifications of the theoretical disc brake squeal model.

2. Model development

The dynamic instability of disc-pad coupled brake system subject to friction stresses on distributed deformable contact surface is investigated. The disc is subject to the clamped boundary condition at the inner radius (a_i) of the rotating shaft with a constant rotating speed, Ω and the free boundary condition at the outer radius (a_o). The homogeneous pad is modeled with free boundary conditions at all edges. It is assumed that the pad is loaded and supported under the uniform pressure pressed by the rigid caliper (or its piston). Fig. 1 describes the system configuration and coordinate systems to be used in the analysis.

The disc and pads are connected with linear contact stiffness (k_c) of the friction material in the manner that one end of the contact stiffness is fixed to the pad contact surface and the other end is in contact with the disc surface in the Z direction. A uniform contact pre-stress (p_o) is symmetrically applied over the contact area on both sides of the rotating disc. Figs. 2 and 3 illustrate the contact kinematics described on the currently deformed surfaces of the disc and pads. $\mathbf{r_a}$ and $\mathbf{u_a}$ are the position and displacement vectors of the perturbed

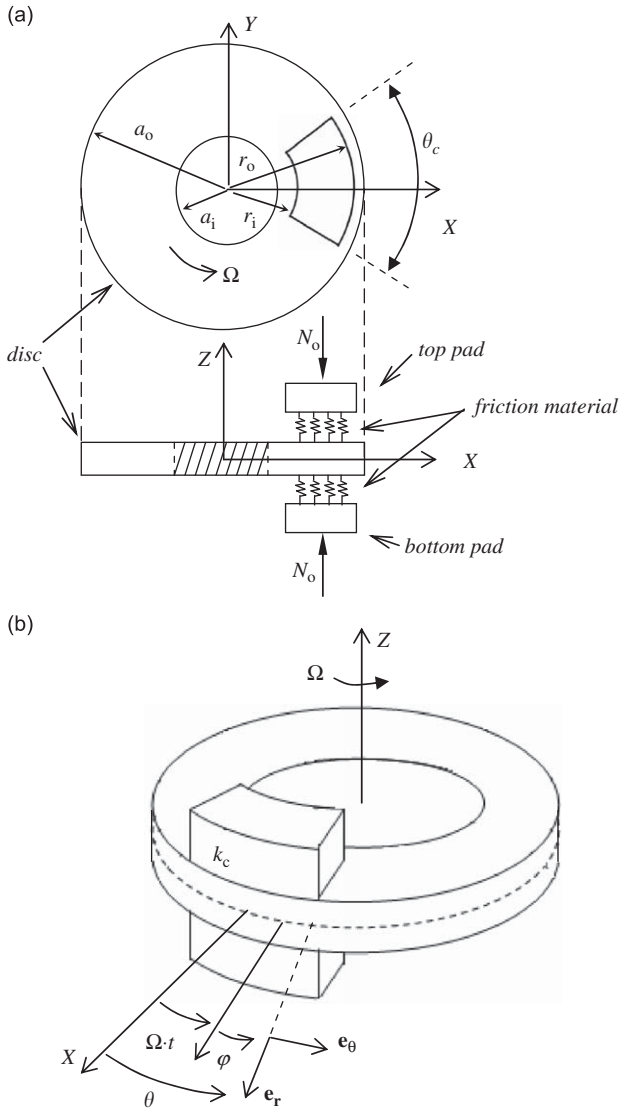

Fig. 1. Rotating disc and two stationary flexible pads: (a) model configuration; (b) reference (r,θ) and local (r,φ) coordinates; $N_o = p_o \times$ (contact area).

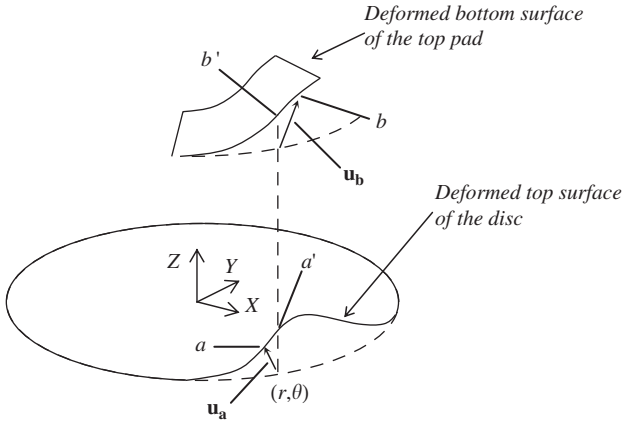

Fig. 2. Description of contact locations, a' and b'at (r,θ) in current configuration.

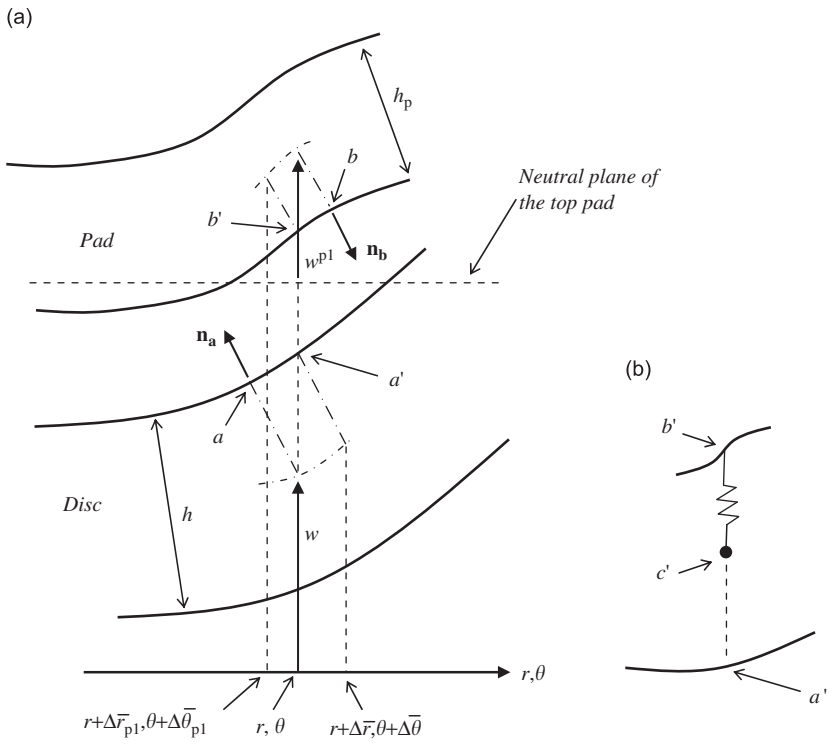

Fig. 3. Contact kinematics in 2D figure: (a) deformation of the disc and the top pad; (b) friction material in contact with the disc at a' and c'.

contact position a of the disc. $\mathbf{u_b}$ is the displacement vector of the perturbed contact position b of the top pad. $\mathbf{n_a}$ and $\mathbf{n_b}$ are unit normal vectors on the surfaces of the disc and top pad. a' and c' are in contact at current time t, where $\langle \mathbf{r_{b'}}, \mathbf{e_r} \rangle = \langle \mathbf{r_{c'}}, \mathbf{e_r} \rangle$ and $\langle \mathbf{r_{b'}}, \mathbf{e_\theta} \rangle = \langle \mathbf{r_{c'}}, \mathbf{e_\theta} \rangle$ for all time and $\langle \cdot, \cdot \rangle$ denotes the inner product. Here, the transverse displacement of the disc is denoted as $\tilde{w}$ in the local coordinates (r,φ) and w in the reference coordinates (r,θ). w^{p1} is the transverse displacement of the top pad.

The contact displacement of the disc at a in Figs. 2 and 3 take the form:

$$\mathbf{u_a} = \mathbf{r_a} - \left(r \cdot \mathbf{e_r} + \frac{h}{2}\mathbf{e_z} \right), \tag{2}$$

where

$$\mathbf{r_a} = r \cdot \mathbf{e_r} + \tilde{w}(r, \varphi, t)\mathbf{e_z} + \frac{h}{2}\mathbf{n_a}, \tag{3}$$

$$\mathbf{n_a} = \frac{\nabla \mathbf{f_a}}{|\nabla \mathbf{f_a}|}, \tag{4}$$

$$\nabla \mathbf{f_a} = \mathbf{e_z} - \frac{\partial \tilde{w}}{\partial r}\mathbf{e_r} - \frac{\partial \tilde{w}}{r\partial \varphi}\mathbf{e_\theta}. \tag{5}$$

Here the linearized contact model for a thin annular plate [17] is applied such that the contact displacement, $\mathbf{u}_{a'}$ of the disc at a' can be linearly found from $\mathbf{u_a}$ at a by Taylor expansion with the perturbed steps, $\Delta\bar{r}$ and $\Delta\bar{\varphi}$:

$$\mathbf{u}_{a'} = \mathbf{u_a} + \frac{\partial \mathbf{u_a}}{\partial r}\Delta\bar{r} + \frac{\partial \mathbf{u_a}}{\partial \varphi}\Delta\bar{\varphi} + \text{h.o.t.}, \tag{6}$$

$$\Delta\bar{r} = \frac{h}{2}\frac{\partial \tilde{w}(r, \varphi, t)}{\partial r} + \text{h.o.t.}, \tag{7}$$

$$r\Delta\bar{\varphi} = \frac{h}{2}\frac{\partial \tilde{w}(r, \varphi, t)}{r\partial \varphi} + \text{h.o.t.}, \tag{8}$$

where h.o.t. denotes higher order terms. Similarly, the displacement vector of the contact stiffness (friction material) of the top pad at c' is expressed as the following by definition:

$$\mathbf{u}_{c'} = \langle \mathbf{u}_{b'}, \mathbf{e_r}\rangle \mathbf{e_r} + \langle \mathbf{u}_{b'}, \mathbf{e_\theta}\rangle \mathbf{e_\theta} + \langle \mathbf{u}_{a'}, \mathbf{e_z}\rangle \mathbf{e_z}, \tag{9}$$

where

$$\mathbf{u}_{b'} = \mathbf{u_b} + \frac{\partial \mathbf{u_b}}{\partial r}\Delta\bar{r}_{p1} + \frac{\partial \mathbf{u_b}}{\partial \theta}\Delta\bar{\theta}_{p1} + \text{h.o.t.}, \tag{10}$$

$$\mathbf{u_b} = \frac{h_p}{2} \cdot \frac{\partial w^{p1}}{\partial r}\mathbf{e_r} + \frac{h_p}{2r} \cdot \frac{\partial w^{p1}}{\partial \theta}\mathbf{e_\theta} + w^{p1}\mathbf{e_z} + \text{h.o.t.} \tag{11}$$

$$\Delta\bar{r}_{p1} = -\frac{h_p}{2}\frac{\partial w^{p1}(r, \theta, t)}{\partial r} + \text{h.o.t.}, \tag{12}$$

$$r\Delta\bar{\theta}_{p1} = -\frac{h_p}{2}\frac{\partial w^{p1}(r, \theta, t)}{r\partial \theta} + \text{h.o.t.} \tag{13}$$

The velocity vector of the rotating disc at the perturbed position, a corresponding to (r, θ) of the unperturbed neutral plane is obtained by the time-derivative in the reference coordinates (Fig. 1b):

$$\mathbf{V_a} = \frac{D\mathbf{r_a}}{Dt}, \tag{14}$$

where the coordinate transformation is given by the differentiation in the local coordinates (Fig. 1b) such that:

$$\frac{D\tilde{w}(r, \varphi, t)}{Dt} = \frac{\partial w(r, \theta, t)}{\partial t} + \Omega \cdot \frac{\partial w(r, \theta, t)}{\partial \theta}. \tag{15}$$

Again, the velocity at a' of the disc is obtained from Taylor expansion such that:

$$\mathbf{V}_{a'} = \mathbf{V_a} + \frac{\partial \mathbf{V_a}}{\partial r}\Delta\bar{r} + \frac{\partial \mathbf{V_a}}{\partial \theta}\Delta\bar{\theta} + \text{h.o.t.} \tag{16}$$

The velocity vector at c' of the stationary top pad is simply the partial time derivative of the displacement vector at c' such that:

$$\mathbf{V}_{c'} = \frac{\partial \mathbf{u}_{c'}}{\partial t}. \tag{17}$$

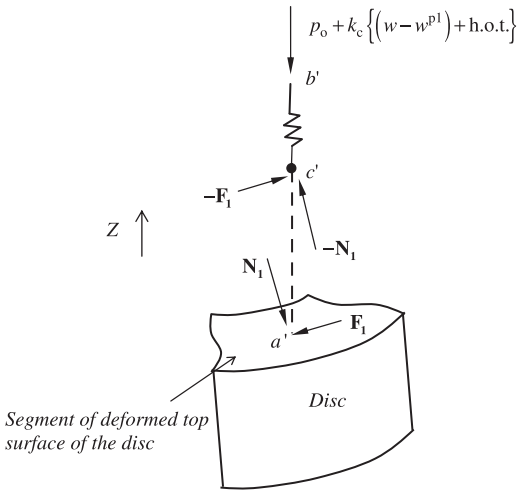

Fig. 4. Contact stresses at a' and c' in current configuration.

Consequently, the direction vector of the relative velocity at the current contact locations, a', c' in the reference coordinates (r, θ) can be expressed in the linearized form at the steady-sliding equilibrium by taking Taylor expansion up to the 1st order such that:

$$\mathbf{d}(f_i) = \mathbf{d}|_{f_i=0} + \sum_{i=1}^{N_f} \left[\left. \frac{\partial\{\mathbf{d}(f_i)\}}{\partial f_i} \right|_{f_i=0} \cdot f_i(r, \theta, t) \right] + \text{h.o.t.} \tag{18}$$

where f_i and N_f are the system variables and the number of variables, respectively, of:

$$\mathbf{d} = \frac{\mathbf{V}_{\mathbf{a}'} - \mathbf{V}_{\mathbf{c}'}}{|\mathbf{V}_{\mathbf{a}'} - \mathbf{V}_{\mathbf{c}'}|}. \tag{19}$$

The friction and normal stresses acting at a' (Fig. 4) are given by:

$$\mathbf{F} = -\mu_1 \cdot N_1 \cdot \mathbf{d}, \tag{20}$$

$$\mathbf{N_1} = -N_1 \cdot \mathbf{n}_{\mathbf{a}'}, \tag{21}$$

where

$$\mathbf{n}_{\mathbf{a}'} = \mathbf{n}_{\mathbf{a}} + \frac{\partial \mathbf{n}_{\mathbf{a}}}{\partial r} \Delta\bar{r} + \frac{\partial \mathbf{n}_{\mathbf{a}}}{\partial \theta} \Delta\bar{\theta} + \text{h.o.t.} \tag{22}$$

The force balance on a single contact spring element in Z direction provides the following relationships:

$$\begin{Bmatrix} N_1 \\ |\mathbf{F_1}| \end{Bmatrix} = \begin{Bmatrix} p_o + k_c(w - w^{p1}) - \frac{\mu_1 p_o}{r} \frac{\partial w}{\partial \theta} + \text{h.o.t.} \\ \mu_1 N_1 \end{Bmatrix} \tag{23}$$

Here the friction–speed relationship is proposed as the function of the relative velocity [25] such that:

$$\mu_1(r, t) = \mu_k + (\mu_s - \mu_k) \cdot e^{-\alpha|\mathbf{V}_{\mathbf{a}'} - \mathbf{V}_{\mathbf{c}'}|}, \tag{24}$$

where μ_s, μ_k and α are the control parameters determining the magnitude and the slope of the friction coefficient.

The virtual work and strain energy by the contact stresses over the top contact area are expressed as:

$$\delta W_{\text{top}} = \int_{-\theta_c/2}^{\theta_c/2} \int_{r_i}^{r_o} \{\langle(-\mathbf{N_1} - \mathbf{F}_1), \delta\mathbf{u}_{\mathbf{c}'}\rangle + \langle(\mathbf{N_1} + \mathbf{F_1}), \delta\mathbf{u}_{\mathbf{a}'}\rangle\} \cdot r \, dr \, d\theta, \tag{25}$$

$$U_{\mathrm{c,top}} = \frac{k_{\mathrm{c}}}{2}\int_{-\theta_{\mathrm{c}}/2}^{\theta_{\mathrm{c}}/2}\int_{r_{\mathrm{i}}}^{r_{\mathrm{o}}}(\langle \mathbf{u}_{\mathbf{b}'}, \mathbf{e}_{\mathbf{z}}\rangle - \langle \mathbf{u}_{\mathbf{c}'}, \mathbf{e}_{\mathbf{z}}\rangle)^2 \cdot r\,dr\,d\theta, \tag{26}$$

where θ_{c}, r_{i} and r_{o} are the contact arc angle, the inner and outer radii, respectively, of the contact area, and where $\mathbf{u}_{\mathbf{a}'}$ and $\mathbf{u}_{\mathbf{c}'}$ are expanded up to 2nd order from Eqs. (6) and (9). Similarly, the virtual work and contact strain energy on the bottom contact are derived as well. Therefore, the total virtual work and contact strain energy of this disc brake system are obtained from:

$$\delta W = \delta W_{\mathrm{top}} + \delta W_{\mathrm{bottom}}, \tag{27}$$

$$U_{\mathrm{c}} = U_{\mathrm{c,top}} + U_{\mathrm{c,bottom}} \tag{28}$$

From the discretization of Lagrange equations by modal coordinates, the friction-coupled equations of motion are given by:

$$\frac{d}{dt}\left[\frac{\partial L}{\partial \dot{a}_m}\right] - \frac{\partial L}{\partial a_m} = \sum_{n=1}^{N} Q_{mn}(a_n), \quad m = 1, \ldots, N, \tag{29}$$

$$L = T - (U + U_{\mathrm{c}}), \tag{30}$$

where U is the total strain energy of the disc and two pads, and

$$T = T_{\mathrm{p1}} + T_{\mathrm{d}} + T_{\mathrm{p2}}, \tag{31}$$

$$T_{\mathrm{d}} = \frac{1}{2}\rho h\int_0^{2\pi}\int_{a_{\mathrm{i}}}^{a_{\mathrm{o}}}\left[\frac{\partial w(r,\theta,t)}{\partial t} + \Omega\frac{\partial w(r,\theta,t)}{\partial \theta}\right]^2 \cdot r\,dr\,d\theta, \tag{32}$$

$$T_{\mathrm{p1}} = \frac{1}{2}\rho_{\mathrm{p}} h_{\mathrm{p}}\int_{-\theta_{\mathrm{c}}/2}^{\theta_{\mathrm{c}}/2}\int_{r_{\mathrm{i}}}^{r_{\mathrm{o}}}\left[\frac{\partial w^{\mathrm{p1}}(r,\theta,t)}{\partial t}\right]^2 r\,dr\,d\theta, \tag{33}$$

$$T_{\mathrm{p2}} = \frac{1}{2}\rho_{\mathrm{p}} h_{\mathrm{p}}\int_{-\theta_{\mathrm{c}}/2}^{\theta_{\mathrm{c}}/2}\int_{r_{\mathrm{i}}}^{r_{\mathrm{o}}}\left[\frac{\partial w^{\mathrm{p2}}(r,\theta,t)}{\partial t}\right]^2 r\,dr\,d\theta, \tag{34}$$

$$\delta W \equiv \sum_{m=1}^{N}\sum_{n=1}^{N} Q_{mn}(a_n)\cdot \delta a_m. \tag{35}$$

Here, p1 and p2 denote the top and bottom pads and the modal coordinates, $\mathbf{a} = \{\underline{q}^{\mathrm{p1}}\ \ \underline{q}\ \ \underline{q}^{\mathrm{p2}}\}^{\mathrm{T}}$ correspond to the disc and two pad modes.

The transverse displacement of the disc is discretized by the first $N_{\mathrm{d}}/2$ eigenfunctions of a stationary disc [23]:

$$w(r,\theta,t) = \sum_{n=1}^{N_{\mathrm{d}}/2} R_n(r)\cdot\{\cos n\theta\cdot q_{2n-1}(t) + \sin n\theta\cdot q_{2n}(t)\}, \tag{36}$$

where $\{R_n(r)\}_{n=1,\ldots,N_{\mathrm{d}}/2}$ is the radial eigenfunction with the nth nodal diameter described by Bessel functions. Approximations to the flexible mode shapes of the pad are obtained by the Rayleigh–Ritz method. The rigid body modes of the pad are found using a geometric calculation of the mass moments of inertia for the pad. As a result, the transverse displacement of the top and bottom pad, respectively, can be rewritten from Refs. [21,24] in the modal expansion form:

$$w^{\mathrm{p1}}(r,\theta,t) = \sum_{k=1}^{N_{\mathrm{p}}} W_k(r,\theta)\cdot q_k^{\mathrm{p1}}(t), \tag{37}$$

$$w^{p2}(r,\theta,t)=\sum_{k=1}^{N_p} W_k(r,\theta)\cdot q_k^{p2}(t), \tag{38}$$

where $\{W_k(r,\theta)\}_{k=1,\ldots,N_p}$ is the kth mode shape of the pad including both flexible and rigid body modes, and N_p is the number of truncated pad modes. The rigid modes of the pad are obtained by small angle approximation and their second order terms are neglected in Eqs. (25) and (26). The total number of the modes used in the disc-pad coupled model is $N=N_d+2N_p$. Substituting Eqs. (36)–(38) along with the normalization relations of $\rho h\pi\int_{a_i}^{a_o} R_n^2\cdot r\,dr\equiv 1$ and $\rho_p h_p\int_{-\theta_c/2}^{\theta_c/2}\int_{r_i}^{r_o}(W_k^2)r\,dr\,d\theta\equiv 1$ into Eqs. (32)–(34) provide the following equations of motion:

$$\ddot{\mathbf{a}}+(\mathbf{G}+\mathbf{D})\dot{\mathbf{a}}+(\mathbf{K_s}+\mathbf{K_{ns}})\mathbf{a}=\mathbf{0}, \tag{39}$$

where all matrices are $N\times N$ and arise from virtual work terms in Appendix A in the following form:

$$\mathbf{D}=\mathbf{C}+\mathbf{R_d}+\mathbf{N_s}, \tag{40}$$

$$\mathbf{K_s}=\mathbf{diag}(\omega_n^2)+\mathbf{A}+\mathbf{P}, \tag{41}$$

$$\mathbf{K_{ns}}=\mathbf{B}+\mathbf{F}. \tag{42}$$

Here $\mathbf{G}(=-\mathbf{G}^T)$, $\mathbf{C}(=2\xi_n\cdot\mathbf{diag}(\omega_n))$, $\mathbf{R_d}(=\mathbf{R_d^T})$ and $\mathbf{N_s}(=\mathbf{N_s^T})$ are the gyroscopic, structural modal damping, radial dissipative, and friction-slope matrices, respectively. ω_n is the undamped natural frequencies of the uncoupled disc and pad components. $\mathbf{A}(=\mathbf{A}^T)$ and $\mathbf{P}(=\mathbf{P}^T)$ are the contact stiffness and pre-load stiffness matrices within the symmetric stiffness matrix. In the non-symmetric stiffness matrix, $\mathbf{B}(\neq\mathbf{B}^T)$ is the non-symmetric non-conservative work matrix produced by friction couple. The additional non-symmetric matrix, $\mathbf{F}(\neq\mathbf{F}^T)$ represents the non-conservative work due to frictional follower forces on the disc and pad contact surface.

In the stiffness matrix, the effect of **P** and **F** on the squeal propensity of disc brake system is of concern because the FE method of commercial disc brake system including these effects has not been developed. It is important to note that **P** and **F** are eliminated if the contact stress is defined on the undeformed surface of the disc without rotation. **A** and **B** have been developed from the disc-pad coupled system with contact forces defined on the undeformed disc surfaces [21–24]. Here the symmetric stiffness matrix **A** determines the frequencies of the coupled system with respect to the contact stiffness between the disc and pads. The non-symmetric stiffness matrix **B** has been found to be a principal destabilizing component in coupled-mode stability analysis [15,21–24]. $\mathbf{R_d}$ was found to stabilize the friction-engaged disc with decreasing speed [17]. The contribution of **G**, $\mathbf{N_s}$, **P** and **F** is yet to be addressed.

A key issue is to provide a physical interpretation of the comprehensive equations of motion (39). This task is not merely to determine the overall stability of steady sliding in the system, but to conduct analytical investigation for the contribution of physical parameters to the onset of instability. For this purpose, the system is simplified to a reduced-order model. A one-doublet mode model [23] can be used for providing the comprehensive perspective on binary flutter in the linear squeal analysis.

3. Stability analysis and results

3.1. The reduced-order model: single-doublet mode approximation

For this work, the pad is assumed to be stationary and rigid, and Eq. (39) is reduced for a single-doublet mode pair (sine and cosine modes) such that:

$$w(r,\theta,t)=R_n(r)\cdot\{\cos(n\theta)\cdot a_{2n-1}+\sin(n\theta)\cdot a_{2n}\}. \tag{43}$$

By applying the single-doublet modal expansion (43) to Eq. (39), the reduced system matrices for the nth one-doublet mode pair is constructed in the following (2×2) matrix form:

$$\mathbf{G}=\begin{bmatrix}0 & g\\ -g & 0\end{bmatrix}, \tag{44}$$

$$\mathbf{C}=2\xi_n\omega_n\begin{bmatrix}1 & 0\\ 0 & 1\end{bmatrix}, \tag{45}$$

$$\mathbf{R_d}=\begin{bmatrix}R_{d1} & 0\\ 0 & R_{d2}\end{bmatrix}, \tag{46}$$

$$\mathbf{N_s}=\begin{bmatrix}N_{s1} & 0\\ 0 & N_{s2}\end{bmatrix}, \tag{47}$$

$$\mathbf{K_s}=\begin{bmatrix}\Omega_1^2 & 0\\ 0 & \Omega_2^2\end{bmatrix}, \tag{48}$$

$$\mathbf{K_{ns}}=\begin{bmatrix}0 & b_1\\ b_2 & 0\end{bmatrix}, \tag{49}$$

where $g=2n\Omega$ is the gyroscopic coupling term, Ω_1 and Ω_2 are the circular natural frequencies of the stiffness-coupled system ($k_c\neq 0,\mu=0$) and each component of the matrices is described in Appendix B. Here, the non-symmetric stiffness elements, b_1 and b_2 are the essential part reflecting the frictional mode-coupling between two modes subject to both the non-conservative friction couple and the frictional follower force loading. The linear stability of the system with the matrices of Eqs. (44)–(49) is qualitatively investigated in terms of binary flutter in the following.

3.2. The stability criterion

The Routh–Hurwitz criterion is applied for the following characteristic equation of the single-doublet mode model of the disc brake system:

$$\lambda^4+c_1\lambda^3+c_2\lambda^2+c_3\lambda+c_4=0, \tag{50}$$

where

$$c_1=D_1+D_2, \tag{51}$$

$$c_2=\Omega_1^2+\Omega_1^2+D_1D_2+g^2, \tag{52}$$

$$c_3=D_2\Omega_1^2+D_1\Omega_2^2-(b_2-b_1)g, \tag{53}$$

$$c_4=\Omega_1^2\Omega_2^2-b_1b_2 \tag{54}$$

$$D_1=2\xi_n\omega_n+R_{d1}+N_{s1}, \tag{55}$$

$$D_2=2\xi_n\omega_n+R_{d2}+N_{s2}, \tag{56}$$

with D_1 and D_2 assumed to be positive. From (B.7) and (B.8), $b_1>0$ and $b_2<0$ automatically result in:

$$c_i>0,\quad i=1,2,3,4. \tag{57}$$

The necessary and sufficient conditions for stability take the form:

$$c_1c_2 - c_3 > 0, \tag{58}$$

$$(c_1c_2 - c_3)c_3 - c_1^2c_4 > 0. \tag{59}$$

From Eqs. (58)–(59) and Eqs. (C.1) and (C.2) of Appendix C, instability occurs for damping approaching zero ($D_1 \to +0$ and $D_2 \to +0$) and $g \neq 0$ when either of the following conditions is met:

$$\lim_{D_1,D_2\to+0}(c_1c_2 - c_3) \to -(b_1 - b_2)g < 0, \tag{60}$$

$$\lim_{D_1,D_2\to+0}\{(c_1c_2 - c_3)c_3 - c_1^2c_4\} \to -\{(b_1 - b_2)g\}^2 < 0. \tag{61}$$

These indicate that the friction-engaged doublet modes without damping are always destabilized by the gyroscopic term since the frictional mode-coupling between a doublet mode pair is non-zero and non-conservative ($b_1 \neq b_2$). Therefore, the friction-coupled binary modes are subject to gyroscopic destabilization. It will be further examined by the perturbation method in the later section.

On the other hand, the influences of damping on stability can be seen by letting $g = 0$ and expressing the stability conditions (58) and (59) in the perturbation form of $\varepsilon_o(\equiv D_1)$ and $\varepsilon_d(\equiv D_2 - D_1)$ as described in Eqs. (C.3) and (C.4) of Appendix C. For the case of $\varepsilon_d \to 0$, the instability occurs when:

$$\lim_{\varepsilon_d\to0}[\{(\Omega_1^2 - \Omega_2^2)^2 + 4b_1b_2\} + 2(\Omega_1^2 + \Omega_2^2)\varepsilon_o^4] < 0. \tag{62}$$

From this, it is seen that the flutter instability for a stationary disc requires: $(\Omega_1^2 - \Omega_2^2)^2 + 4b_1b_2 < 0$ (which is also referred to as the mode-coupling instability [23,24]), where the absolute value (ε_o) of the damping coefficient can effectively stabilize the system. In contrast, the difference between modal damping (ε_d) becomes a destabilizing factor such that the instability for the case of $\varepsilon_o \to 0$ arises when:

$$\lim_{\varepsilon_o\to0}\{(c_1c_2 - c_3)c_3 - c_1^2c_4\} = b_1b_2\varepsilon_d^2 < 0. \tag{63}$$

Since $b_1b_2 < 0$, due to the frictional mode-coupling of the doublet mode pair, the non-zero ε_d contributes to the instability which is called the "damping instability [26]" or the "smooting effect [27]". It is concluded from Eqs. (60)–(63) that destabilization is associated with $(b_1 - b_2)g$ and b_1b_2 which will be referred to as the gyroscopic frictional mode-coupling and the stationary frictional mode-coupling, respectively.

In the automotive application, the contact stiffness of a friction material is much larger than the actual brake pressure-related term, ($k_c \gg p_o \cdot h/r^2$) as referred to Tables 2 and 3, and Refs. [14–16]. From this, it will be shown that the contributions of $(b_1 - b_2)g$ and b_1b_2 to the flutter instability highly depend upon the choice of point or distributed contact modeling. Moreover, since the point contact approximation has been proposed by several authors [9,14] and [16,17] for the purpose of simplification, it is relevant in this point to discuss about the validity of this approximation. Table 1 summarizes the order of the two frictional mode-coupling terms incorporated into two different contact models: the distributed-loaded contact and its point contact approximation. The major difference between the concentrated point and distributed-loaded contact models is the order of the stationary frictional mode-coupling, b_1b_2. In the point contact model, the necessary condition

Table 1
Order of frictional mode-coupling and frequency separation.

Contact model	b_1, b_2	$(b_1 - b_2)g$	b_1, b_2	$(\Omega_1^2 - \Omega_2^2)^2$
Concentrated-point contact	$b_1 \sim O(k_c)$ $b_2 \sim O(p_o \cdot h/r^2)$	$O(g \cdot k_c)$	$O(k_c \cdot p_o \cdot h/r^2)$	$O(k_c^2)$
Distributed-loaded contact	$b_1 \sim O(k_c)$ $b_2 \sim O(k_c)$	$O(g \cdot k_c)$	$O(k_c^2)$	$O(k_c^2)$

Table 2
Nominal values of disc parameters.

Parameter	Symbol	Value
Outer radius of disc	a_o	150 mm
Inner radius of disc	a_i	90 mm
Young's modulus	E	88.9 GPa
Density of disc	ρ	7150 kg m^{-3}
Poisson ratio	v	0.285
Thickness of disc	h	13.0 mm

Table 3
Nominal values of pad parameters.

Parameter	Symbol	Value
Outer radius of contact	r_o	142 mm
Inner radius of contact	r_i	100 mm
Contact angle	θ_c	62°
Young's modulus	E_p	207 GPa
Density of pad	ρ_p	7820 kg m^{-3}
Poisson ratio	v_p	0.29
Thickness of pad	h_p	8.0 mm
Pre-load	N_o	2000 N
Nominal contact stiffness	k_{nom}	0.35×10^{11} N m^{-3}

for mode-coupling type instability (due to the stationary frictional mode-coupling) cannot be met since:

$$(\Omega_1^2 - \Omega_2^2)^2 + 4b_1b_2 = O(k_c^2) - O(k_c \cdot p_o \cdot h/r^2) \gg 0. \tag{64}$$

Instead, the major mechanism producing the dynamic instability in the point contact model becomes the gyroscopic frictional mode-coupling, $(b_1 - b_2)g \cong 2n\Omega \cdot b_1$ found from Eqs. (60) and (61), where one of the dominant system parameters is the disc rotation speed. In contrast, the distributed friction stresses in the distributed-loaded contact model can generate the sufficient amount of the stationary frictional mode-coupling satisfying $4b_1b_2 < -(\Omega_1^2 - \Omega_2^2)^2$, where b_1b_2 is highly influenced by the system geometry such as θ_c and k_c [23,24]. The subsequent analytical and numerical analysis will be based on the distributed-loaded contact model as described in Tables 2 and 3, where the rotation effects will be considered.

As discussed earlier, the pre-stress terms in the stiffness matrix are much smaller than the contact stiffness terms ($k_c \gg p_o \cdot h/r^2$). Particularly, the frictional follower forces rarely contribute to the dynamic instability due to the domination of friction couples on both of $(b_1 - b_2)g$ and b_1b_2 in the single-doublet mode model. The statement is shown to be valid for the multiple-mode model as well. In the multiple-mode equations of motion of Eq. (39), **F** and **P** can be seen to contribute little to system stiffness matrix due to the dominating role of **B** and **A**. From Eq. (39), the eigensolutions of the system with and without pre-stress terms **F** and **P** in the stiffness matrix are separately calculated and their positive real part loci are drawn in the same figure (Fig. 5). In this plot, the difference between the two sets of results is not visible since they are virtually identical. From this, it can be concluded that the contact modeling defined on the undeformed surfaces of the disc can provide good approximate stability solutions for a car disc brake system.

From the Routh–Hurwitz stability criterion applied on the reduced-order model, the contributions of frictional mode-coupling terms, $(b_1 - b_2)g$ and b_1b_2 to the instability have been summarized in terms of the order of system parameters. However, the eigensolutions are required to provide the better qualitative explanation on squeal propensity. The closed-form solutions of Eq. (50) for two special cases are provided and the general solution of Eq. (50) is numerically calculated in the following.

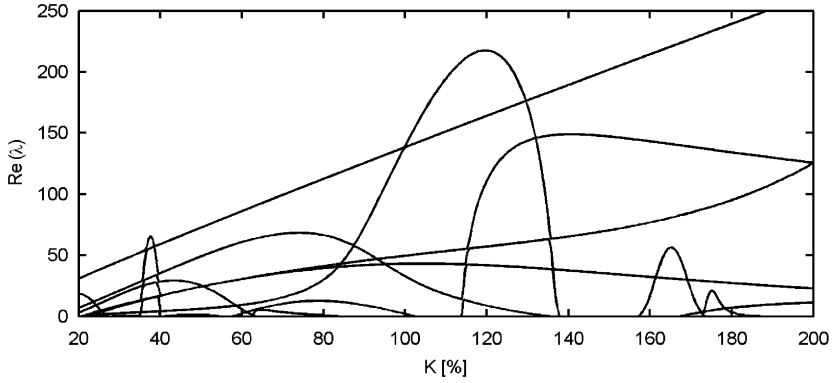

Fig. 5. Positive real part loci of disc-pad system ($N=38$) with and without pre-stress terms in the stiffness matrix for $\Omega=5\,\mathrm{rad\,s^{-2}}$, $\mu=0.5$ and $K[\%]=100\cdot k_c/k_{nom}$; the real part loci of two solutions are virtually identical.

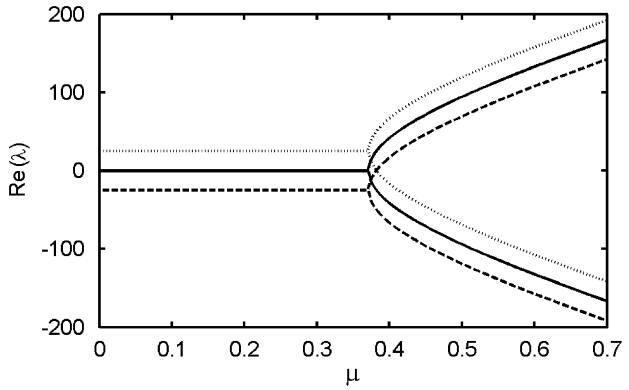

Fig. 6. The effects of b_1b_2 and $\varepsilon_o(=D)$ on the binary instability for case 1 ($g=0, \varepsilon_d=0$); (—) for $D=0.0$, (----) for $D=50.0$, (…) for $D=-50.0$, $n=7$; b_1b_2 generates the splitting in Re(λ) and ε_o changes Re(λ) regardless of μ.

Case 1. $D\equiv D_1=D_2$, $g=0$ (no gyroscopic effect)

In the absence of the gyroscopic term g with identical modal damping coefficients ($\varepsilon_d=0$ and $\varepsilon_o=D$), the eigensolution of Eq. (50) becomes:

$$\lambda=-D/2\pm\frac{1}{2}\sqrt{D^2-2(\Omega_1^2+\Omega_2^2)\pm2\sqrt{(\Omega_1^2-\Omega_2^2)^2+4b_1b_2}}. \tag{65}$$

For $D^2\ll2(\Omega_1^2+\Omega_2^2)$, Eq. (65) is approximated by:

$$\lambda\cong-D/2+\lambda_U, \tag{66}$$

where λ_U is the eigenvalue of the undamped system [23]:

$$\lambda_U=\pm\frac{1}{2}\sqrt{-2(\Omega_1^2+\Omega_2^2)\pm2\sqrt{(\Omega_1^2-\Omega_2^2)^2+4b_1b_2}} \tag{67}$$

λ_U possesses the positive real parts with non-zero frequencies (flutter instability) only when $(\Omega_1^2-\Omega_2^2)^2+4b_1b_2<0$, implying that Re($\lambda_U$) splits into positive and negative branches when $(\Omega_1^2-\Omega_2^2)^2+4b_1b_2<0$ (Fig. 6). Here the damping factor, D of Eq. (66) shifts the entire loci of Re(λ) negatively with an increase in D. Moreover, the stationary frictional mode-coupling ($b_1b_2<0$) is shown to be essential in producing the binary flutter.

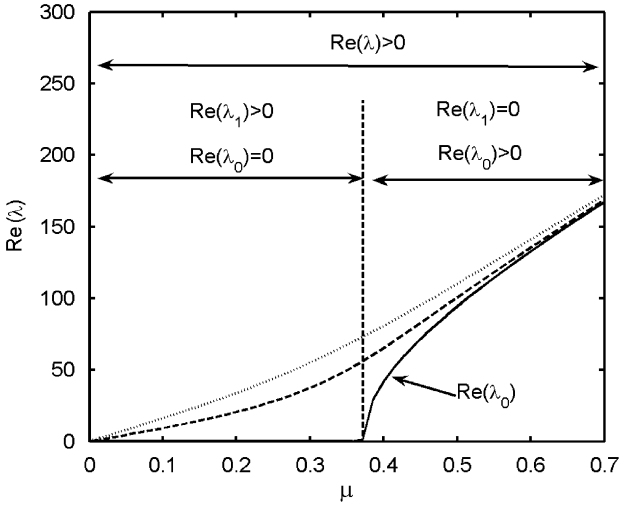

Fig. 7. The effects of b_1b_2 and $(b_1-b_2)g$ on the binary instability for case 2 ($\varepsilon_o=\varepsilon_d=0$); (—) for $\Omega=0.0$, (- - - -) for $\Omega=5.0\,\mathrm{rad\,s^{-1}}$, (…) for $\Omega=10.0\,\mathrm{rad\,s^{-1}}$, $n=7$; b_1b_2 generates the splitting in $\mathrm{Re}(\lambda_0)$ and $(b_1-b_2)g$ strengthens the splitting of $\mathrm{Re}(\lambda_0)$.

Case 2. $D_1=D_2=0$, $g\neq 0$ (gyroscopic effect without damping)

In the second case, the effect of the gyroscopic term g is assessed in the absence of damping. The corresponding undamped characteristic equation takes the form:

$$\lambda^4+(\Omega_1^2+\Omega_2^2+g^2)\lambda^2+(b_1-b_2)g\lambda+(\Omega_1^2\cdot\Omega_2^2-b_1b_2)=0. \tag{68}$$

A straightforward perturbation method is applied where the gyroscopic term and the eigensolution are expressed by the perturbation parameter, ε:

$$g=\varepsilon\cdot g_o, \tag{69}$$

$$\lambda=\lambda_0+\varepsilon\cdot\lambda_1+O(\varepsilon^2). \tag{70}$$

By substituting Eqs. (69) and (70) into Eq. (68), the set of equations corresponding to the order of ε are given by:

$$\varepsilon^0:\lambda_0^4+(\Omega_1^2+\Omega_2^2)\lambda_0^2+(\Omega_1^2\cdot\Omega_2^2-b_1b_2)=0 \tag{71}$$

$$\varepsilon^1:\lambda_0^2\lambda_1+2(\Omega_1^2+\Omega_2^2)\lambda_1+(b_1-b_2)g_o=0, \tag{72}$$

which result in:

$$\lambda_0=\pm\frac{1}{2}\sqrt{-2(\Omega_1^2+\Omega_2^2)\pm 2\sqrt{(\Omega_1^2-\Omega_2^2)^2+4b_1b_2}}, \tag{73}$$

$$\lambda_1=\pm g_o(b_1-b_2)/\sqrt{(\Omega_1^2-\Omega_2^2)^2+4b_1b_2}, \tag{74}$$

where λ_0 is identical to λ_U of Eq. (67) associated with the stationary frictional mode-coupling (b_1b_2). $_1$ is the correction factor for the single-doublet mode model subject to gyroscopic loading. The singular case of λ_1 at $(\Omega_1^2-\Omega_2^2)^2+4b_1b_2=0$ is not within the scope of this paper.

From Eq. (74), it is found that $\mathrm{Re}(\lambda_1)$ has both of the positive and negative branches at $(\Omega_1^2-\Omega_2^2)^2+4b_1b_2>0$, whereas they coalesce to zero when $(\Omega_1^2-\Omega_2^2)^2+4b_1b_2<0$. Therefore, the coalescing point of $\mathrm{Re}(\lambda_1)$ is identical with the split point of $\mathrm{Re}(\lambda_0)$ in such a manner that $\mathrm{Re}(\lambda_1)=0$ and $\mathrm{Re}(\lambda_1)>0$ correspond to $\mathrm{Re}(\lambda_0)>0$ and $\mathrm{Re}(\lambda_0)=0$, respectively, as described in Fig. 7. Since the two branches of $\mathrm{Re}(\lambda)$ are smoothly split, it can be also called the ''smoothing effect'' attributed to the gyroscopic frictional mode-coupling. The general description of the smoothing effect on a circulatory system can be referred to [28].

Equivalently, the gyroscopic frictional mode-coupling, $(b_1 - b_2)g_o$ in Eq. (74) contributes to the positive real parts of Eq. (70) in the order of ε^1 for $\mathrm{Re}(\lambda_0) = 0$ and at most $O(\varepsilon^2)$ for $\mathrm{Re}(\lambda_0) > 0$. It indicates that the non-zero rotation speed associated with g_o guarantees the dynamic instability if $(b_1 - b_2)g_o \neq 0$ for the undamped binary mode pair. In summary, the stationary and gyroscopic frictional mode-coupling effects can contribute to the binary flutter of a doublet mode pair in the order of ε^0 and ε^1, respectively, depending on system parameters.

Case 3. $D_1 \neq D_2$, $g \neq 0$ (general disc operational case)

The exact eigensolution of Eq. (50) is now numerically determined and interpreted on the basis of the perspectives obtained from the approximate analytical solutions. The radial dissipative effect, known to be proportional to $1/\Omega$, is seen to be effective at low speeds as shown in Figs. 8a and b. Since the radial dissipative terms (R_{d1}, R_{d2}) are also proportional to μ, the entire loci of the real parts rotate clockwise around the pivot point ($\mu = 0$), leading to the decrease of $\mathrm{Re}(\lambda)$. This will be called the "tilting effect". Besides, the non-equally structural damping in the coupled modes (without the radial dissipative and negative friction-slope terms) has been found to have the destabilizing "smoothing effect" [26–29]. In this doublet mode model, the structural damping coefficients of the doublet mode pair are assumed to be identical. Since the radial dissipative terms of the disc cosine and sine modes produce the overall separation of their modal damping coefficients as in Eqs. (B.1) and (B.2), however, the "smoothing effect" caused by the non-equal damping is involved as well. Therefore, it is concluded that the two branches of $\mathrm{Re}(\lambda)$ of the undamped disc doublet modes undergo some modification due to the "smoothing effect" of the gyroscopic term and both the "tilting and smoothing effects" of the radial dissipative terms.

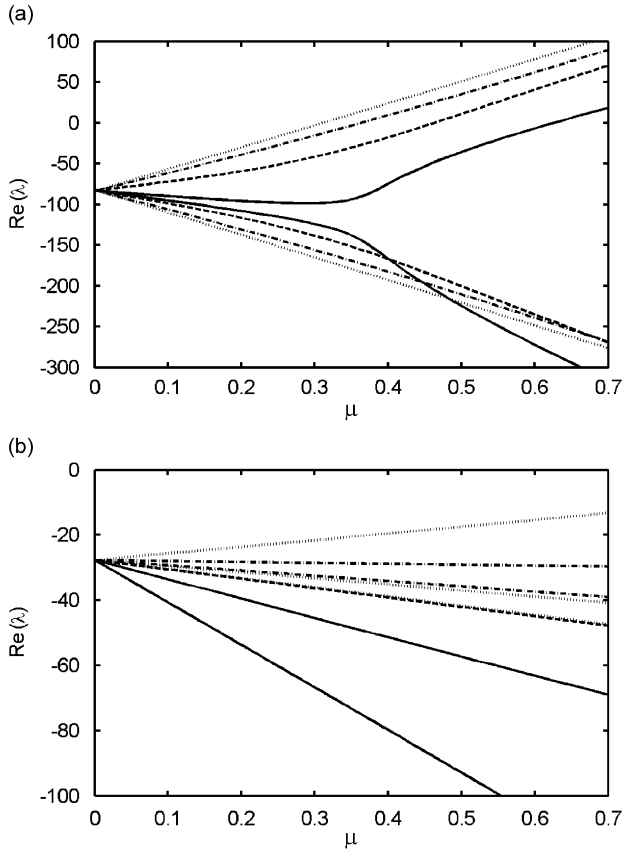

Fig. 8. The effects of $b_1 b_2$, $(b_1 - b_2)g$ and physical damping (D_1, D_2) on the binary instability of the structurally damped system ($\xi_n = 0.002$); (a) $n = 7$ ($\mathrm{Re}(\lambda_0)$ loci split near $\mu = 0.4$), (b) $n = 2$ ($\mathrm{Re}(\lambda_0) = 0$ up to $\mu = 0.7$); (—): $\Omega = 2.0\,\mathrm{rad\,s^{-1}}$, (- - - -): $\Omega = 8.0\,\mathrm{rad\,s^{-1}}$, (- · -): $\Omega = 20\,\mathrm{rad\,s^{-1}}$, (…): $\Omega = 50\,\mathrm{rad\,s^{-1}}$.

The major difference between Figs. 8a and b is that the 7th doublet mode ($n = 7$) retains mode-coupling type instability ($\mathrm{Re}(\lambda_0) > 0$), but the 2nd doublet mode ($n = 2$) does not ($\mathrm{Re}(\lambda_0) = 0$). Here, the binary instability can be stated in terms of rotation speed and mode-coupling type instability as the followings. For the mode pair having zero $\mathrm{Re}(\lambda_0)$, high rotation speed is required for $\mathrm{Re}(\lambda) > 0$. For the mode pair with $\mathrm{Re}(\lambda_0) > 0$, however, the positive $\mathrm{Re}(\lambda)$ can arise more easily even at low speeds.

In application to the automotive brake squeal problem, the rotation speed can be considered to be low and the braking system will have structural damping. Therefore, the stationary frictional mode-coupling ($b_1 b_2$) determining $\mathrm{Re}(\lambda_0)$ is the essential part as stated in Figs. 7 and 8. Since $b_1 b_2$ is shown to depend on the contact area in Table 1, a brake model should have the distributed-loaded contact model not to miss this substantial squeal source. Although this conclusion is based on the reduced-order model, it will be shown in the next section that it is also valid for a multiple degree-of-freedom model. Hereafter, the flutter instability of the multiple-mode model is numerically investigated, where the 12 modes (6 rigid and 6 vibration modes) of each pad and the 20 disc vibration modes are used in the multiple-mode model.

3.3. Stability results based on constant friction coefficient

Tseng and Wickert [11] investigated the stability of a rotating disc subject to the distributed frictional follower force. They demonstrated that $\mathrm{Re}(\lambda)$ of the non-conservative gyroscopic system is influenced by Ω over the broad range of speed (beyond the critical speed). In automotive applications, however, the squeal analysis on the non-conservative gyroscopic brake system is limited to low speeds. For this, Hochlenert et al. [17] and Ouyang and Mottershead [19] used a slowly-rotating annular plate and showed that the squeal propensity is proportional to the increase of the rotation speed under the constant friction coefficient.

As mentioned in the previous sections, the squeal propensity of the mode-coupled modes under rotation effect should be investigated by using a disc brake model with finite contact area. The one doublet mode model has shown that $\mathrm{Re}(\lambda)$ of a non-conservative gyroscopic brake system is perturbed from that of the system without dissipative and gyroscopic effects with respect to Ω. The radial dissipative term in a dissipative matrix normally decreases $\mathrm{Re}(\lambda)$ as stated in Eq. (66), where the radial dissipative effect is inversely proportional to Ω. In contrast, the gyroscopic term increases $\mathrm{Re}(\lambda)$ due to the gyroscopic frictional mode-coupling $g_o(b_1 - b_2)$ of Eq. (74) which is proportional to Ω. As a result, there is a certain speed $\bar{\Omega}$ corresponding to the cancellation of

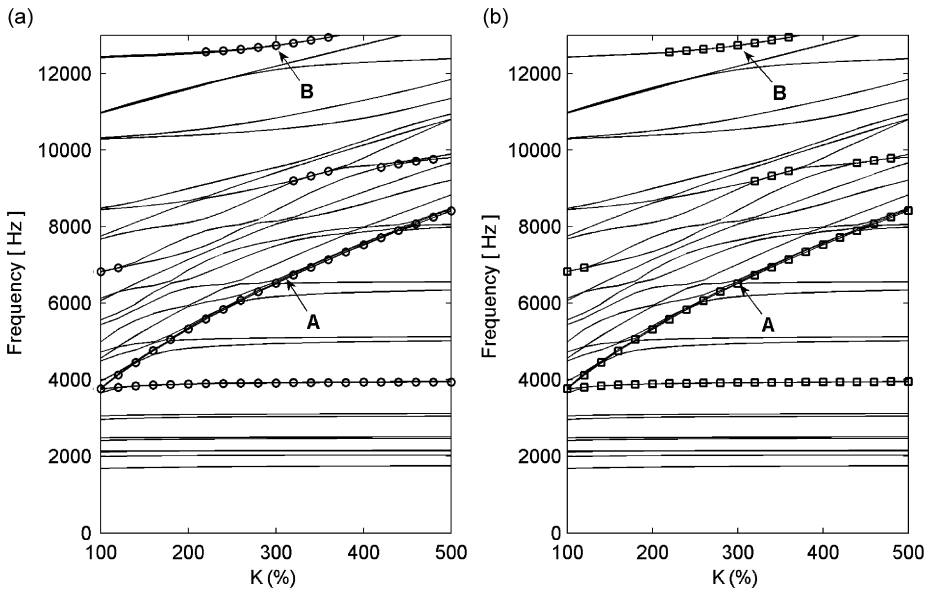

Fig. 9. Modal stability boundaries ($N = 38$) for constant $\mu(= 0.5)$; the occurrence of the positive real parts with respect to k_c is marked on the frequency loci by (a) (○) for the rotating disc model, (b) (□) for the rotation-free disc model, $\Omega = 5\,\mathrm{rad\,s^{-1}}$ and $\xi_n = 0.002$.

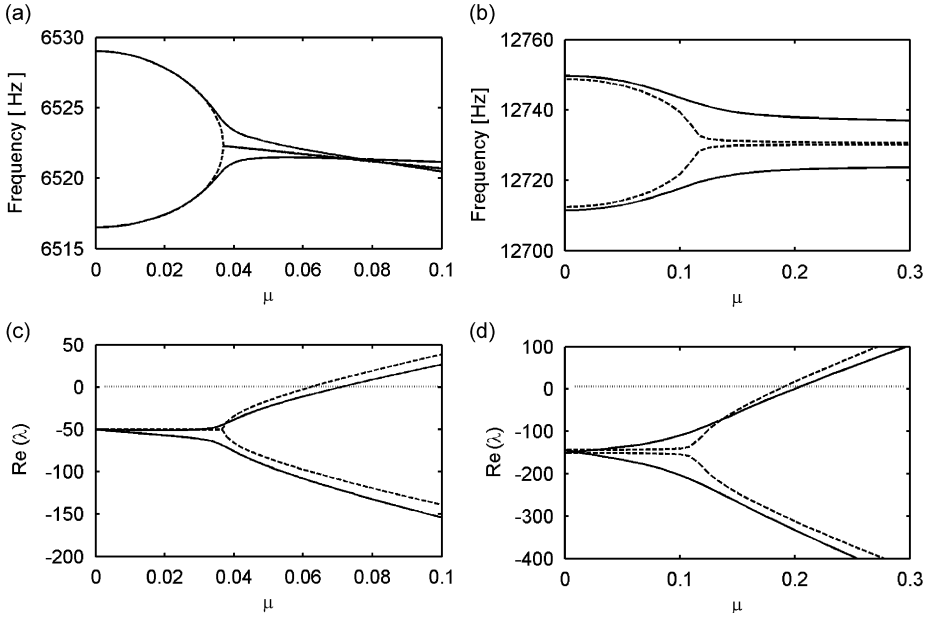

Fig. 10. flutter modes for the rotating disc (—) and the rotation-free disc (- - - -) at $K = 300(\%)$ in $\mu - \text{Hz}$ domain, (a) mode "**A**", (b) mode "**B**", and $\mu - \text{Re}(\lambda)$ domain (c) mode "**A**", (d) mode "**B**".

these rotation effects on $\text{Re}(\lambda)$. This will be shown to be applicable for the multiple-mode model as well in the following.

At $\bar{\Omega}$, it is assumed that the rotation effects are diminished in the multiple-mode model, resulting in the following equations of motion neglecting rotation-dependent elements in Eq. (39):

$$\ddot{\mathbf{a}} + \mathbf{C}\dot{\mathbf{a}} + (\mathbf{K}_s + \mathbf{K}_{ns})\mathbf{a} = \mathbf{0}, \tag{75}$$

where the eigensolutions provide the mode-coupling instability ($\text{Re}(\lambda_0) > 0$) caused by the stationary frictional mode-coupling. It will be referred to as the rotation-free model. The further simplification can be done by neglecting **P** and **F** of Eqs. (41) and (42) as stated in Eq. (39). Figs. 9a and b illustrate the flutter modes ($\text{Re}(\lambda) > 0$) on their frequency loci (at $\mu = 0.5$) over the range of contact stiffness for both the rotating and rotation-free disc brake model. The stability boundaries of the flutter modes in the rotation-free model are seen to approximate those found from the rotating disc model at $\Omega = 5\,\text{rad}\,\text{s}^{-1}$. It indicates that the rotation-free disc approximation is valid in determining stability boundaries of the rotating disc brake near certain speeds which are normally low-to-moderate speeds. Therefore, Eq. (75) is an approximate set of equations of motion to be used for the prediction of the flutter instability of a rotating disc brake with distributed contact stresses near the certain speed $\bar{\Omega}$. It should be noted that the rotation-free model is the disc brake model with circumferential friction force in the absence of gyroscopic terms and the radial component of friction force.

Two of the flutter modes in Fig. 9 are chosen for investigating the rotation effect on squeal propensity. The eigenvalues of mode "**A**" and mode "**B**" in Fig. 9 are shown as functions of friction coefficient in Fig. 10. In the $\mu - \text{Re}(\lambda)$ domain (Figs. 10c and d), the critical value of μ for squeal with and without rotation effects are found to be close.

From Figs. 9 and 10, two aspects are to be highlighted. The first aspect is the rotation-free disc approximation as discussed in Fig. 9. The second aspect is that the stationary frictional mode-coupling mainly contributes to the flutter instability. Since the rotation effects are seen to be insignificant in destabilizing the system, the stationary frictional mode-coupling is the dominant destabilizing factor in causing the splitting of the real part loci, and therefore, resulting in the flutter instability of the disc brake system ($\text{Re}(\lambda) > 0$).

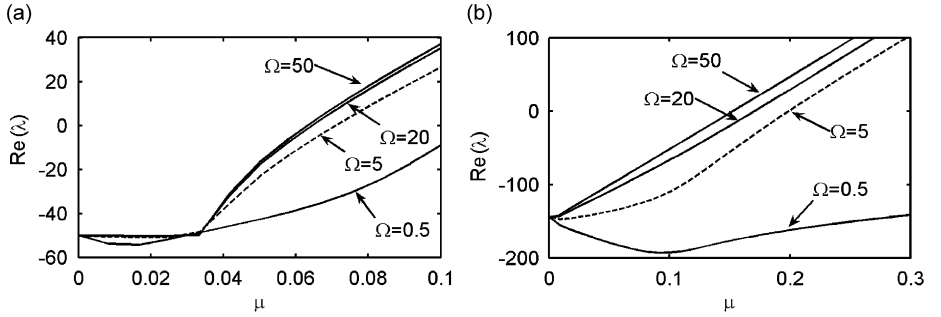

Fig. 11. The higher Re(λ) of pair loci with respect to Ω [rad/s] for the flutter modes in Fig. 9, (a) mode "**A**", (b) mode "**B**".

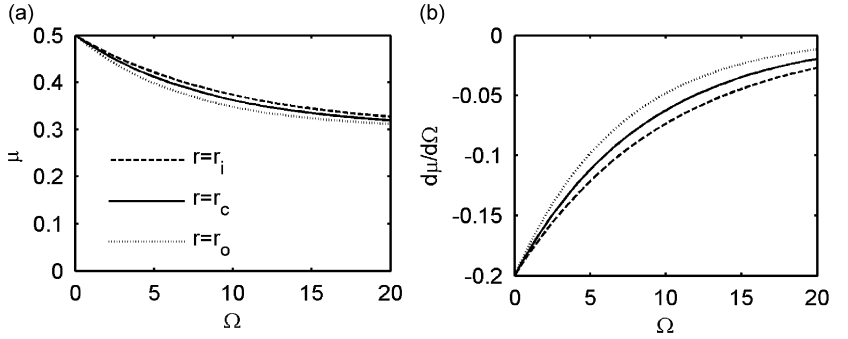

Fig. 12. Friction curves, (a) friction coefficient, $\mu_s = 0.5$, $\mu_k = 0.3$, $\alpha = 1$, (b) the slope of friction coefficient, $r_c = 116\,\text{mm}$.

Fig. 11 illustrates the influence of the rotation speed on the real parts of eigenvalues. At low-to-moderate speeds in the automotive application, the rotation effects change the squeal onset (Re(λ) = 0) little. At the very low speeds, however, the rotation effects effectively contribute to the stabilization of system equilibrium, and therefore, the rotation-free disc approximation is not appropriate. It is notable that the stabilization associated with rotation speed arises from the radial component of friction stresses in such a way that the dissipative effect of radial friction is proportional to $1/\Omega$.

3.4. Stability results based on rotation-dependent friction coefficient

The previous numerical results of the multiple-mode model were based on the constant friction coefficient, where the radial dissipative and gyroscopic destabilizing effects were discussed as the rotation effects. From these previous results, the propensity for flutter instability was seen to grow with increasing the rotation speed as depicted in Fig. 11. However, the friction coefficient in disc brake system is rather a function of the rotation speed as shown by a brake dynamometer test in Ref. [30]. If friction coefficient is the speed-dependent function as shown in Fig. 12a, the squeal propensity for rotation speed may be altered. Moreover, the negative slope corresponding to friction coefficient in Fig. 12b is shown to change with respect to rotation speed. As a result, the magnitude and slope of the friction coefficient will appear as one of the rotation effects.

It has been found that Re(λ) is influenced by destabilizing factors such as the stationary frictional mode-coupling (mode-coupling type), gyroscopic frictional mode-coupling and negative slope effects, and stabilizing factors such as the structural modal damping and radial dissipative effects. Consequently, the eigenvalues are dependent of the disc rotation speed as depicted in Fig. 13. In this figure, the real part loci of mode "**A**" and mode "**B**" are seen to increase as the disc rotation speed decreases up to certain speeds. Below the certain speeds, the squeal propensity of mode "**A**" and mode "**B**" decreases. Here, the real part of the mode "**B**" drop below $\Omega = 2.5\,\text{rad}\,\text{s}^{-1}$. However, the squeal propensity of the mode "**A**" continues to grow with the decrease of rotation speed nearly up to zero rotation speed.

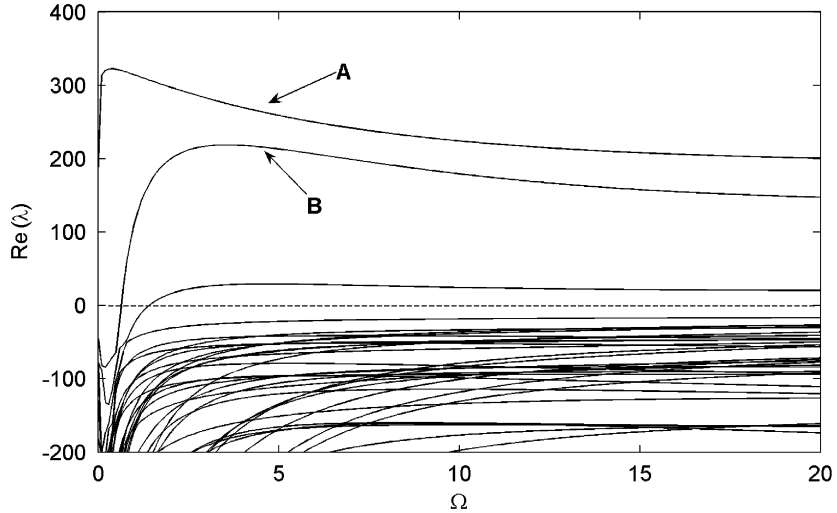

Fig. 13. Rotation-dependent system eigenvalues of disc-pad coupled system with friction curve.

4. Conclusions and discussion

A friction-engaged disc brake system becomes non-conservative due to frictional mode-coupling among system modes and the negative slope of friction coefficient with respect to sliding speed. The frictional mode-coupling originates from the friction couple and the frictional follower force. While the friction couple is the moment produced by the circumferential component of friction force, the frictional follower force is literally the loading generated by the direction change of friction force due to the disc rotation and deformation. In automotive applications, the non-conservative frictional mode-coupling mostly stems from the friction couple, and the contribution of the frictional follower force is negligible. From above, the contact model of describing the contact kinematics on the undeformed surfaces of the disc and pad is considered one practical approximation for contact modeling.

The single-doublet mode model has been used to show that the non-conservative frictional mode-coupling can be classified as either the stationary or gyroscopic frictional mode-coupling. The stationary frictional mode-coupling generates the mode-merging type instability found to be the substantial brake squeal mechanism, whereas the gyroscopic frictional mode-coupling makes the supplementary influence on the mode-coupling destabilization. This paper has shown that the contact stresses should be defined over the true contact area, and not as point contact, in order to capture the stability character arising from the stationary frictional mode-coupling.

From the analytical and numerical investigations on squeal propensity for rotation speed presented here, the steady sliding at the contact surface is shown to be stabilized on the verge of stop due to the dissipative nature of the radial slip. For low-to-moderate speeds, the radial dissipative effect is diminished, and the stationary frictional mode-coupling and the rotation destabilizing effects dominate the equilibrium instability. It is notable that the rotation-free disc brake model can predict the approximate equilibrium instability of the rotating disc brake model at low-to-moderate speeds under the assumption of constant friction coefficient.

For a comprehensive predictive model, the actual relationship between μ and sliding speed should be considered. The other rotation effect arises from the negative slope of μ that is derived by linearizing the friction curve. The numerical results of this comprehensive model have shown that there is a speed corresponding to maximum squeal propensity for each flutter mode.

Appendix A. The virtual work terms per area on the top contact associated with system matrices

$$\mathbf{R_d} : \frac{\mu_1 p_o}{r\Omega}(-\dot{u}^{p1} + \dot{u})\delta(u^{p1} - u), \tag{A.1}$$

$$\mathbf{N_s} : \mu_1 p_o \delta(v^{p1} - v), \tag{A.2}$$

$$\mathbf{P} : \frac{p_o}{h/2}[(1+\mu_1^2)v\delta(v^{p1}-v) + u\delta(u^{p1}-u)], \tag{A.3}$$

$$\mathbf{B} : \mu_1 k_c(-w^{p1}+w)\delta(v^{p1}-v), \tag{A.4}$$

$$\begin{aligned}\mathbf{F} : \mu_1 p_o \Bigg[& \frac{\partial u}{r\partial\theta}\delta(u^{p1}-u) - \left(\frac{\partial v^{p1}}{\partial r} + \frac{v^{p1}}{r}\right)\delta u^{p1} + \left(\frac{\partial v}{\partial r} + \frac{v}{r}\right)\delta u - \left(\frac{u^{p1}}{r} + \frac{\partial v^{p1}}{r\partial\theta}\right)\delta v^{p1} \\ & + \left(\frac{u}{r} + \frac{\partial v}{r\partial\theta}\right)\delta v - u^{p1}\delta\left(\frac{\partial v^{p1}}{\partial r}\right) + u\delta\left(\frac{\partial v}{\partial r}\right) - \frac{v^{p1}}{r}\delta\left(\frac{\partial v^{p1}}{\partial\theta}\right) + \frac{v}{r}\delta\left(\frac{\partial v}{\partial\theta}\right)\Bigg],\end{aligned} \tag{A.5}$$

where $v \equiv \langle \mathbf{u_a}, \mathbf{e_\theta} \rangle$, $v^{p1} \equiv \langle \mathbf{u_b}, \mathbf{e_\theta} \rangle$, $u \equiv \langle \mathbf{u_a}, \mathbf{e_r} \rangle$ and $u^{p1} \equiv \langle \mathbf{u_b}, \mathbf{e_r} \rangle$.

Appendix B. The elements of the one-doublet mode model

$$R_{d1} = \frac{2p_o}{\Omega}\left(\frac{h}{2}\right)^2 \int_{r_i}^{r_o} \left(\frac{\partial R_n}{\partial r}\right)^2 \mu^*(r)\,\mathrm{d}r \cdot \int_{-\theta_c/2}^{\theta_c/2} \cos^2 n\theta\, d\theta, \tag{B.1}$$

$$R_{d2} = \frac{2p_o}{\Omega}\left(\frac{h}{2}\right)^2 \int_{r_i}^{r_o} \left(\frac{\partial R_n}{\partial r}\right)^2 \mu^*(r)\,dr \cdot \int_{-\theta_c/2}^{\theta_c/2} \sin^2 n\theta\, d\theta, \tag{B.2}$$

$$N_{s1} = 2p_o\left(\frac{nh}{2}\right)^2 \int_{r_i}^{r_o} \left[\frac{R_n^2}{r} \cdot \left\{\frac{\partial \mu_1}{\partial v_{,t}}\bigg|_{\{f_i\}=0}\right\}\right] dr \cdot \int_{-\theta_c/2}^{\theta_c/2} \sin^2 n\theta\, d\theta, \tag{B.3}$$

$$N_{s2} = 2p_o\left(\frac{nh}{2}\right)^2 \int_{r_i}^{r_o} \left[\frac{R_n^2}{r} \cdot \left\{\frac{\partial \mu_1}{\partial v_{,t}}\bigg|_{\{f_i\}=0}\right\}\right] dr \cdot \int_{-\theta_c/2}^{\theta_c/2} \cos^2 n\theta\, d\theta, \tag{B.4}$$

$$\begin{aligned}\Omega_1^2 = {} & \omega_n^2 - n^2\Omega^2 + 2k_c \int_{r_i}^{r_o} R_n^2(r) r\, dr \cdot \int_{-\theta_c/2}^{\theta_c/2} \cos^2 n\theta\, d\theta \\ & + 2p_o \cdot n^2\left(\frac{h}{2}\right)\left[\int_{r_i}^{r_o} (1+\mu^*(r)^2)\frac{R_n^2}{r}\, dr \cdot \int_{-\theta_c/2}^{\theta_c/2} \sin^2 n\theta\, d\theta\right] \\ & + 2p_o \cdot \left(\frac{h}{2}\right)\left[\int_{r_i}^{r_o} \left(\frac{\partial R_n}{\partial r}\right)^2 r\,\mathrm{d}r \cdot \int_{-\theta_c/2}^{\theta_c/2} \cos^2 n\theta\, d\theta\right],\end{aligned} \tag{B.5}$$

$$\begin{aligned}\Omega_2^2 = {} & \omega_n^2 - n^2\Omega^2 + 2k_c \int_{r_i}^{r_o} R_n^2(r) r\, dr \cdot \int_{-\theta_c/2}^{\theta_c/2} \sin^2 n\theta\, d\theta \\ & + 2p_o \cdot n^2\left(\frac{h}{2}\right)\left[\int_{r_i}^{r_o} (1+\mu^*(r)^2)\frac{R_n^2}{r}\, dr \cdot \int_{-\theta_c/2}^{\theta_c/2} \cos^2 n\theta\, d\theta\right] \\ & + 2p_o \cdot \left(\frac{h}{2}\right)\left[\int_{r_i}^{r_o} \left(\frac{\partial R_n}{\partial r}\right)^2 r\, dr \cdot \int_{-\theta_c/2}^{\theta_c/2} \sin^2 n\theta\, d\theta\right],\end{aligned} \tag{B.6}$$

$$b_1 = 2n \cdot k_c\left(\frac{h}{2}\right)\left\{\int_{r_i}^{r_o} \mu^*(r) \cdot R_n^2(r)\, dr \cdot \int_{-\theta_c/2}^{\theta_c/2} \sin^2 n\theta\, d\theta\right\} + 2p_o \cdot n^3\left(\frac{h}{2}\right)^2\left[\int_{r_i}^{r_o} \mu^*(r)\left(\frac{R_n}{r}\right)^2 dr \cdot \int_{-\theta_c/2}^{\theta_c/2} \cos^2 n\theta\, d\theta\right] + 2p_o \cdot \left(\frac{h}{2}\right)^2\left[\int_{r_i}^{r_o} \mu^*(r)\left\{-n^3\left(\frac{R_n}{r}\right)^2 + n\left(\frac{\partial R_n}{\partial r}\right)^2\right\} dr \cdot \int_{-\theta_c/2}^{\theta_c/2} \sin^2 n\theta\, d\theta\right] \tag{B.7}$$

$$b_2 = -2n \cdot k_c\left(\frac{h}{2}\right)\int_{r_i}^{r_o} \mu^*(r) \cdot R_n^2(r)\, dr \cdot \int_{-\theta_c/2}^{\theta_c/2} \cos^2 n\theta\, d\theta - 2p_o \cdot n^3\left(\frac{h}{2}\right)^2\left[\int_{r_i}^{r_o} \mu^*(r)\left(\frac{R_n}{r}\right)^2 dr \cdot \int_{-\theta_c/2}^{\theta_c/2} \sin^2 n\theta\, d\theta\right] + 2p_o \cdot \left(\frac{h}{2}\right)^2\left[\int_{r_i}^{r_o} \mu^*(r)\left\{n^3\left(\frac{R_n}{r}\right)^2 - n\left(\frac{\partial R_n}{\partial r}\right)^2\right\} dr \cdot \int_{-\theta_c/2}^{\theta_c/2} \cos^2 n\theta\, d\theta\right] \tag{B.8}$$

where $\mu^* = \mu_1|_{\{f_i\}=0}$ and $v_{,t} = \partial v/\partial t$. Here, the pre-stress p_o terms of Eqs. (B.7) and (B.8) are negligible due to $k_c \gg p_o(h/r^2)$, which results in $b_1 > 0$ and $b_2 < 0$. The stability boundaries with and without the pre-stress terms in the stiffness matrix are virtually identical in the single-doublet mode model and the multiple-mode model as shown in Fig. 5. The pre-stress p_o terms in b_1 and b_2 will be omitted in the stability analysis throughout the paper except Section 3.2 to clarify their contribution on the dynamic instability in terms of the order of system parameters.

Appendix C. The Routh–Hurwitz criterion

$$c_1c_2 - c_3 = \{D_1\Omega_1^2 + D_2\Omega_2^2 + (D_1 + D_2)(D_1D_2 + g^2)\} - (b_1 - b_2)g, \tag{C.1}$$

$$(c_1c_2 - c_3)c_3 - c_1^2c_4 = \{D_1\Omega_1^2 + D_2\Omega_2^2 + (D_1 + D_2)(D_1D_2 + g^2)\} \cdot (D_2\Omega_1^2 + D_1\Omega_2^2) + (D_1 + D_2)^2 \cdot (\Omega_1^2\Omega_2^2 - b_1b_2) + \{D_1\Omega_1^2 + D_2\Omega_2^2 + (D_1 + D_2)(D_1D_2 + g^2)\} \cdot (b_1 - b_2)g - (D_2\Omega_1^2 + D_1\Omega_2^2) \cdot (b_1 - b_2)g - (b_1 - b_2)^2g^2. \tag{C.2}$$

Letting $D_1 \equiv \varepsilon_o(>0)$, $D_2 \equiv \varepsilon_o + \varepsilon_d(>0)$ and $g = 0$, (C.1) and (C.2) are written in the perturbation form of ε_o and ε_d:

$$\begin{aligned} c_1c_2 - c_3 &= \varepsilon_o^0[\varepsilon_d\Omega_2^2] + \varepsilon_o^1[(\Omega_1^2 + \Omega_2^2) + \varepsilon_d^2] + \varepsilon_o^2[3\varepsilon_d] + 2\varepsilon_o^3 \\ &= \varepsilon_d^0[\varepsilon_o(\Omega_1^2 + \Omega_2^2) + 2\varepsilon_o^3] + \varepsilon_d^1[\Omega_2^2 + 3\varepsilon_o^3] + \varepsilon_d^2[\varepsilon_o], \end{aligned} \tag{C.3}$$

$$\begin{aligned} (c_1c_2 - c_3)c_3 - c_1^2c_4 &= \varepsilon_o^0(b_1b_2\varepsilon_d^2) + \varepsilon_o^1[\{(\Omega_1^2 - \Omega_2^2)^2 + 4b_1b_2\}\varepsilon_d + \Omega_1^2\varepsilon_d^3] \\ &\quad + \varepsilon_o^2[\{(\Omega_1^2 - \Omega_2^2)^2 + 4b_1b_2\} + (4\Omega_1^2 + \Omega_2^2)\varepsilon_d^2] + \varepsilon_o^3\{(5\Omega_1^2 + 3\Omega_2^2)\varepsilon_d^2\} \\ &\quad + \varepsilon_o^6(2\Omega_1^2 + 2\Omega_2^2) = \varepsilon_d^0[\{(\Omega_1^2 - \Omega_2^2)^2 + 4b_1b_2\}\varepsilon_o^2 + 2(\Omega_1^2 + \Omega_2^2)\varepsilon_o^6] \\ &\quad + \varepsilon_d^1[\{(\Omega_1^2 - \Omega_2^2)^2 + 4b_1b_2\}\varepsilon_o + (5\Omega_1^2 + 3\Omega_2^2)\varepsilon_o^3] \\ &\quad + \varepsilon_d^2[b_1b_2 + (4\Omega_1^2 + \Omega_2^2)\varepsilon_o^2] + \varepsilon_d^3(\Omega_1^2\varepsilon_o) \end{aligned} \tag{C.4}$$

References

[1] N.M. Kinkaid, O.M. O'Reilly, P. Papadopoulos, Automotive disc brake squeal, *Journal of Sound and Vibration* 267 (2003) 105–166.
[2] H. Ouyang, W. Nack, Y. Yuan, F. Chen, Numerical analysis of automotive disc brake squeal: a review, *International Journal of Vehicle Noise and Vibration* 1 (2005) 207–231.
[3] K. Huseyin, *Vibrations and Stability of Multiple Parameter Systems*, Sijthoff and Noordhoff, Amsterdam, 1978.
[4] S.M. Yang, C.D. Mote, Stability of non-conservative linear discrete gyroscopic systems, *Journal of Sound and Vibration* 147 (3) (1991) 453–464.
[5] J. Li, X. Li, Z. Wang, New theorems on stability of mechanical systems with circulatory forces, *Zeitchrift Angewandte Mathematik Physik* 50 (1999) 839–843.
[6] O.N. Kirillov, Gyroscopic stabilization of non-conservative systems, *Physics Letters A* 359 (3) (2006) 204–210.
[7] O.N. Kirillov, Destabilization paradox due to breaking the Hamiltonian and reversible symmetry, *International Journal of Non-linear Mechanics* 42 (1) (2007) 71–87.
[8] B. Hervé, J.J. Sinou, H. Mahé, L. Jézéquel, Analysis of squeal noise and mode coupling instabilities including damping and gyroscopic effects, *European Journal of Mechanics, A/Solids* 27 (2) (2008) 141–160.
[9] M.R. North, *Disc brake squeal, in: Braking of road vehicles, Automobile Division of the Institution of Mechanical Engineers*, Mechanical Engineering Publications Limited, London, England, 1976, pp. 169–176.
[10] J.E. Mottershead, Vibration and friction induced instability in disks, *The Shock and Vibration Digest* 30 (1998) 14–31.
[11] J.G. Tseng, J.A. Wickert, Nonconservative stability of a friction loaded disk, *Journal of Vibration and Acoustics* 120 (1998) 922–929.
[12] W.V. Nack, A.M. Joshi, Friction induced vibration: brake moan, Technical Report, 951095, *SAE*, Warrendale, PA, 1995.
[13] W.V. Nack, Brake squeal analysis by finite elements, *International Journal of Vehicle Design* 23 (2000) 263–275.
[14] H. Ouyang, J.E. Mottershead, Dynamic instability of an elastic disk under the action of a rotating friction couple, *Journal of Applied Mechanics* 71 (2004) 753–758.
[15] J. Flint, J. Hulten, Lining-deformation-induced modal coupling as squeal generator in a distributed parameter disc brake model, *Journal of Sound and Vibration* 254 (2002) 1–21.
[16] J. Heilig, J. Wauer, Stability of a nonlinear brake system at high operating speeds, *Nonlinear Dynamics* 34 (2003) 235–247.
[17] D. Hochlenert, G.S. Korspeter, P. Hagedorn, Friction induced vibrations in moving continua and their application to brake squeal, *Journal of Applied Mechanics* 74 (2007) 542–549.
[18] H. Ouyang, J.E. Mottershead, D.J. Brookfield, S. James, M.P. Cartmell, A Methodology for the determination of dynamic instabilities in a car disc brake, *International Journal of Vehicle Design* 23 (2000) 241–262.
[19] H. Ouyang, J.E. Mottershead, A bounded region of disc-brake vibration instability, *Journal of Vibration and Acoustics* 123 (2001) 543–545.
[20] S. Kung, G. Stelzer, V. Belsky, A. Bajer, Brake squeal analysis incorporating contact conditions and other nonlinear effects, Technical Report, 2003-01-3343, SAE, Warrendale, PA, 2003.
[21] H.V. Chowdhary, A.K. Bajaj, C.M. Krousgrill, An analytical approach to model disc brake system for squeal prediction. *Proceedings of ASME DETC* 2001, Pittsburgh, September, 9–12.
[22] J. Huang, C.M. Krousgrill, A.K. Bajaj, An efficient approach to estimate critical value of friction coefficient in brake squeal analysis, *Journal of Applied Mechanics* 74 (2007) 534–541.
[23] J.Y. Kang, C.M. Krousgrill, F. Sadeghi, Dynamic instability of a thin circular plate with friction interface and its application to disc brake squeal, *Journal of Sound and Vibration* 316 (2008) 164–179.
[24] J.Y. Kang, C.M. Krousgrill, F. Sadeghi, Analytical formulation of mode-coupling instability in disc-pad coupled system, *International Journal of Mechanical Science* 51 (2009) 52–63.
[25] M.T. Bengisu, A. Akay, Stability of friction-induced vibrations in multi-degree-of-freedom system, *Journal of Sound and Vibration* 171 (4) (1994) 557–570.
[26] N. Hoffmann, L. Gaul, Effects of damping on mode-coupling instability in friction induced oscillations: imperfect merging of modes and viscous instability, *Journal of Applied Mathematics and Mechanics* 83 (2003) 524–534.
[27] G. Fritz, J.J. Sinou, J.M. Duffal, L. Jézéquel, Investigation of the relationship between damping and mode-coupling patterns in case of brake squeal, *Journal of Sound and Vibration* 307 (2007) 591–609.
[28] O.N. Kirillov, A.P. Seyranian, Stabilization and destabilization of a circulatory system by small velocity-dependent forces, *Journal of Sound and Vibration* 283 (2005) 781–800.
[29] J.J. Sinou, L. Jézéquel, Mode coupling instability in friction induced vibrations and its dependency on system parameters including damping, *European Journal of Mechanics A/Solids* 26 (1) (2007) 106–122.
[30] J.Y. Kang, S. Choi, Brake dynamometer model predicting brake torque variation due to disc thickness variation, *Journal of Automobile Engineering* 221 (2007) 49–55.